Universidad Nacional Autónoma de México

Programa de Posgrado en Ciencias Físicas.
Maestría en Ciencias Físicas.

Mie scattering by fatty acid vesicles may have been able to shield early life from dangerous Archean UV-C light

T E S I S

que para optar por el grado de

Maestro en Ciencias (Física)

PRESENTA:
Iván Lechuga Jiménez

Tutor Principal:
Dr. Karo Michaelian Pauw, Instituto de Física, UNAM
Miembros del Comité Tutor: Dr. Octavio Reymundo Miramontes Vidal, Instituto de Física, UNAM
Dr. Iván Santamaría Holek, Facultad de Ciencias, UNAM

México, CDMX. (Agosto) 2023

To those who provided me with love.

Acknowledgments

I'm grateful to the people who have been with me throughout all these processes. A particular thank you to my parents and sister for their unconditional support as well as to the rest of my family and friends. I'm also thankful to my tutor for all these years of mentoring and support. Of course, thanks to my dog and Bad Bunny.

The author acknowledges the financial support of DGAPA - UNAM project number IN104920 and acknowledges CONACyT for a national postgraduate studentship.

Abstract

Theories on the origin of life usually consider the prebiotic vesicles (protocells) as systems with the primary function of compartmentalizing precursor molecules for enhancing the reaction-diffusion chemistry leading to abiogenesis. The vesicle membrane acts as a semi-permeable barrier between the interior of the vesicle and the environment. Based on the evidence indicating that the origin of life was driven by photo-chemical dissipative structuring using the soft UV-C light region (245-275 nm), we have suggested that the fatty acids vesicles could act as Mie UV scatterers providing the molecules of life confined inside them shielding against hard UV-C photons (180-210 nm), which can ionize and dissociate the molecules. Therefore, the shielding could foment the dissipative structuring of those molecules. This protection could have been helpful before the formation of the ozone layer, after the evolution of oxygenic photosynthesis.

Contents

List of Figures

Chapter 1

Introduction

1.1 Thermodynamic Dissipation Theory for the Origin of Life

Theories on the origin of life should consider the physiochemical properties of chemical systems to explain the emergence of life. The "Thermodynamic Dissipation Theory of the Origin and Evolution of Life" (TDTOEL) [3, 12–16] has proposed that life emerged from the dissipative structuring of fundamental molecules of life. It has identified the flux of UV-C photons coming from the early sun during the Archean as the source of free energy for dissipative structuring and evolution of the fundamental molecules, see figure 1.2. This theory has explained the synthesis, proliferation, and selection of the fundamental molecules of life under Archean conditions.

Protocells or prebiotic vesicles are chemical systems recognized as precursors of the first living cells [17]. A protocell consists of a bi-layer membrane of spherical shape containing chemical species in a water solvent. The origin of protocells from the TDTOEL perspective has been addressed elsewhere [4]. In this work, we suggest that the vesicle also constitutes an optical system (figure 2.1) that could have important implications for the origin of life and photon dissipation. We will introduce the general framework of TDTOEL, discuss protocells, the dissipative structuring of fatty acids, vesicle formation, and Mie scattering. Next, we will discuss the simulations of the

vesicle's optics, show the results, and finally, discuss our conclusions.

TDTOEL suggests that the first molecules of life were, in the beginning, UV-pigments dissipatively structured at the ocean surface under the solar photon spectrum before the origin of life ($\sim$ 3.85 Ga); see figure 1.2. A dissipative structure is a non-equilibrium and non-linear system that arises to increase the dissipation rate of an imposed generalized thermodynamic potential. It, therefore, increases the entropy flow into its environment. It evolves through different stationary states with a tendency to reach states of greater dissipation.

To understand dissipative structuring and how these kinds of structures relate to life's origin, it is necessary to discuss some non-equilibrium thermodynamics.

Non-equilibrium thermodynamics, or classical irreversible thermodynamics, deals with open systems. These systems allow the exchange of matter and energy with their environment. Prigogine and collaborators [18] have proposed that the entropy S of an open system changes due to irreversible processes occurring within the system and due to the exchange of entropy between the system and its environment, as is shown by the equation 1.1.

$$\frac{dS}{dt} = \frac{d_i S}{dt} + \frac{d_e S}{dt}, \tag{1.1}$$

where $\frac{d_i S}{dt}$ is the change in the system's entropy due to irreversible internal processes and $\frac{d_e S}{dt}$ is the change due to the flow of entropy over the boundaries. $\frac{d_i S}{dt}$ is also known as entropy production.

According to the second law, $\frac{d_i S}{dt}$ is always positive, whereas $\frac{d_e S}{dt}$ is not restricted. If the flow of entropy from the system to the environment is high enough, the total change of entropy of the system could be negative, allowing for the emergence of order. This process is known as structuring and could correspond to spatial or temporal organization.

Prigogine and collaborators have shown that under the hypothesis of local equilibrium[1] the entropy production can be written as shown in the equation 1.2:

[1] A system out of equilibrium has local equilibrium if each point within it has a macroscopic but small neighborhood which is in equilibrium.

$$\frac{d_i S}{dt} = \sum_k J_k X_k. \tag{1.2}$$

J_k is the flow associated with some irreversible processes k, and X_k is its corresponding generalized force. When the relationship between forces and flows is linear, the system is in a linear regimen. For example, heat conduction is an irreversible process described by a linear relationship between heat flow and a generalized force. During this process, the system always reaches a unique stationary state with minimum entropy production.

Non-linear systems allow the existence of more than one stationary state and do not always evolve towards the one with the minimum entropy production. A bifurcation diagram can represent the multiple available stationary states; see figure 1.1. As seen in the graph, the entropy production becomes a function of some parameter λ; given the variation of this parameter, the system can reach a bifurcation point. At this point, the system becomes sensible to fluctuations and stochastically evolves through one of the possible branches. It has been shown that the evolution of autocatalytic systems, including living systems, is towards states of generally greater dissipation.

Sometimes a non-linear system presents a structuring process through bifurcations and reaches a state with greater dissipation, called a dissipative structure. It dissipates the imposed external thermodynamic generalized potential over the system. A standard example of dissipative structure is the Bénard cell; see figure 1.1. This system consists of two plates separated by a distance L, the bottom plate is at a higher temperature than the top one, and there is fluid between them. The fluid is under the force of gravity. When the temperature difference is such that the Rayleigh number is below its critical value, the system transports heat only by conduction. Still, convection arises within the system when the temperature difference exceeds the critical value. These turbulent states lie in the non-linear regimen, and then the Bénard or convection cell appears. According to Manneville [19], the Bénard cell is an example of a system in a weak turbulent state. A weak turbulent state is a transition state between a laminar state and a turbulent state. In some cases, it has been shown that two possible states arise. First, when the hot fluid flows up from the center of the cell and goes back cool along the borders, and, second, when the hot fluid flows up from the edges and goes

back cool into the center. However, the first one has the highest entropy production and is the most stable and observed.

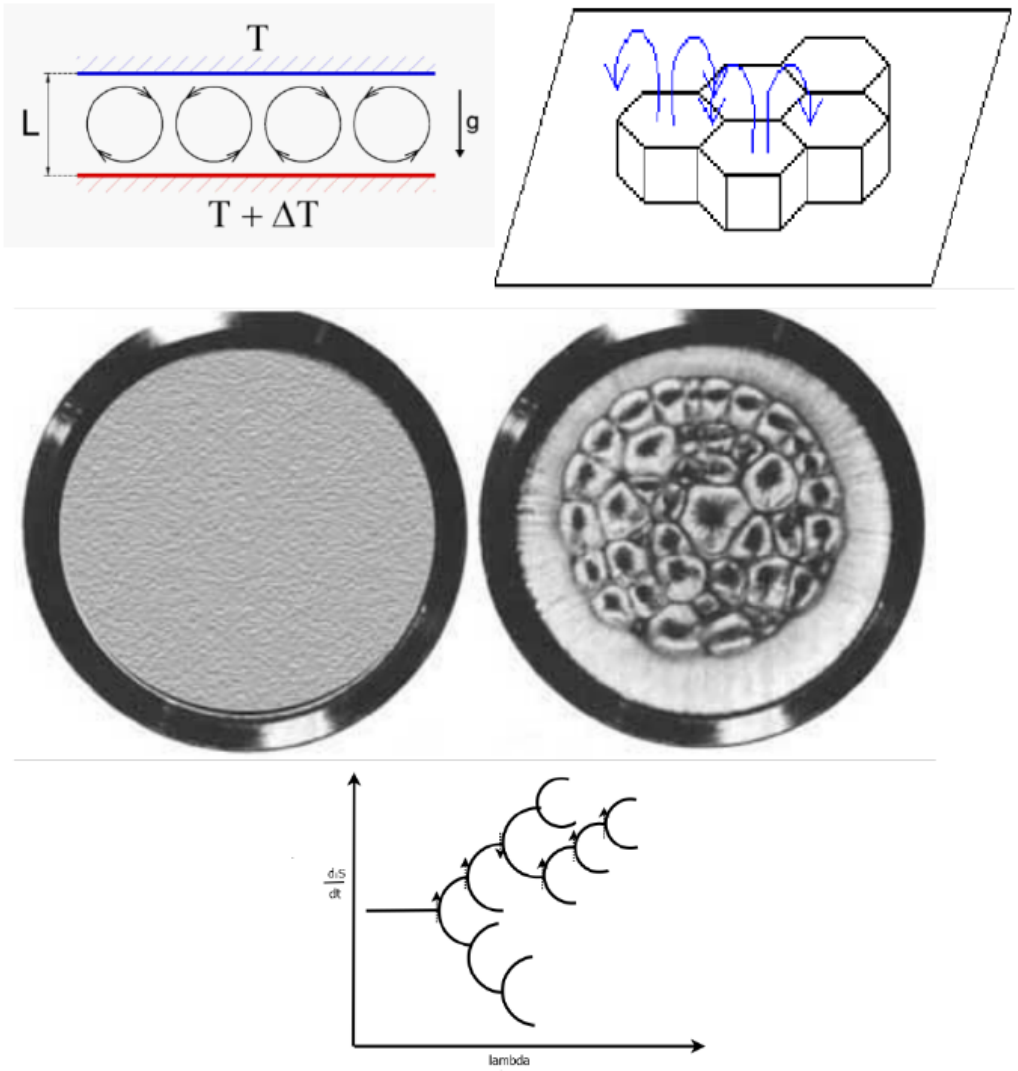

Figure 1.1: Bénard cell and illustrative bifurcation diagram. A non-equilibrium non-linear system can evolve through different states of entropy production; for some states, the evolution could be stochastic. At these points, the system evolves to a possible branch (up and down arrows). The entropy production depends on a parameter λ, which characterizes the system; for a Bénard cell, it is the Rayleigh number. Adapted from [1].

TDTOEL has suggested that the fundamental molecules of life were originally microscopic dissipative structures that arose to dissipate the UV-C photon potential available during the Archean. Further details can be found elsewhere [3–5, 11–16, 20–23].

Three main arguments support the TDTOEL. First, the fundamental molecules of life absorb and dissipate exactly in the UV-C region that was arriving at Earth's surface during the Archean. Secondly, the photochemical routes to the fundamental molecules require simple precursors in water solution and UV-C light. Finally, the fundamental molecules have conical intersections, or affinity to ones with one, which allow for rapid dissipation of the photon-induced excitation energy into heat.

Figure 1.2 shows the names of fundamental molecules of life located at their maximum absorption wavelength. The name of each molecule has a font size proportional to its molar extinction coefficient. They cover the region of 205 to 280 nm (UV-C region). Photons in this region have enough energy to break and remake covalent bonds of carbon-based precursor molecules like HCN and CO_2 in water. Still, they do not have enough energy to ionize and destroy these molecules. This and the fact that these molecules dissipate their excitation energy rapidly into heat suggests that the fundamental molecules of life were pigments dissipatively structured to dissipate UV-C photons.

All of the fundamental molecules of life can be synthesized from single precursors, like HCN and cyanogen, by photochemical routes that use UV-C photons and produce structures with a greater photon dissipation rate. For example, figure 1.3 shows the route for the formation of adenine [15]. Adenine has an absorption peak at 260 nm. The maximum of the UV-C light intensity before the origin of life is located at about the same wavelength. This example shows how these systems evolve through photochemical and chemical reactions to different structures until the final structure has the highest photon dissipation. Other examples can be found elsewhere [24].

All of the fundamental molecules of life have a conical intersection or have a chemical affinity with other molecules that have a conical intersection. The nucleobases of DNA and RNA (adenine, guanine, cytosine, and thymine or uracil) reach an electronically excited state when absorbing UV-C light that decays extremely rapid ($< 2 \times 10^{-12}$s) through internal conversion [25]. In this process, the electronic excitation induces a geometrical transformation of the molecule. In this state, the vibrational state superimposed on the electronically excited states can couple with the vibrational states

superimposed on the electronic ground state. This type of coupling is called a conical intersection. The system decays via the conical intersection, converting the initial photon energy into molecular vibrations (heat). The quantum efficiency of the original excitation transformation into heat is very large and gives the molecule photochemical stability (the energy is dissipated before any other change could be induced in the molecule), but, more importantly, the conical intersection provides the molecule with a high rate of photon dissipation (the photon energy is efficiently transformed into heat). See figure 1.4.

In summary, the postulate of this theory, i.e., the suggestion that fundamental molecules of life were originally UV-C pigments dissipative structured to dissipate the photon potential available before the Archean, is based on three points: that these molecules have strong absorption exactly in the UV-C region, that all of them can be synthesized from photochemical routes parting from precursors molecules (such as H_20, HCN, cyanogen, and CO_2) operating in the UV-C region, and that all of them also have conical intersections leading to a high rate of photon dissipation.

The non-equilibrium thermodynamics have further implications for understanding the origin of life. From the TDTOEL, it has been proposed that the evolution and complexation of life are processes subjected to the fundamental laws of thermodynamics. The thermodynamic imperative of increasing the efficiency of photon dissipation can be seen today, for example, in comparing entropy production of several living materials against non-living ones and in studies about the thermodynamics of ecosystems [16,26]. Therefore, the increase in photon dissipation should be related to the origin of complex biochemical structures at and after the origin of life.

The protocells are chemical systems formed of membranes of bilayers of amphiphilic molecules that were useful as containers for prebiotic chemistry. The role of these systems from a photon dissipative perspective is a primary concern for the TDTOEL. The following section discusses the protocells' general properties.

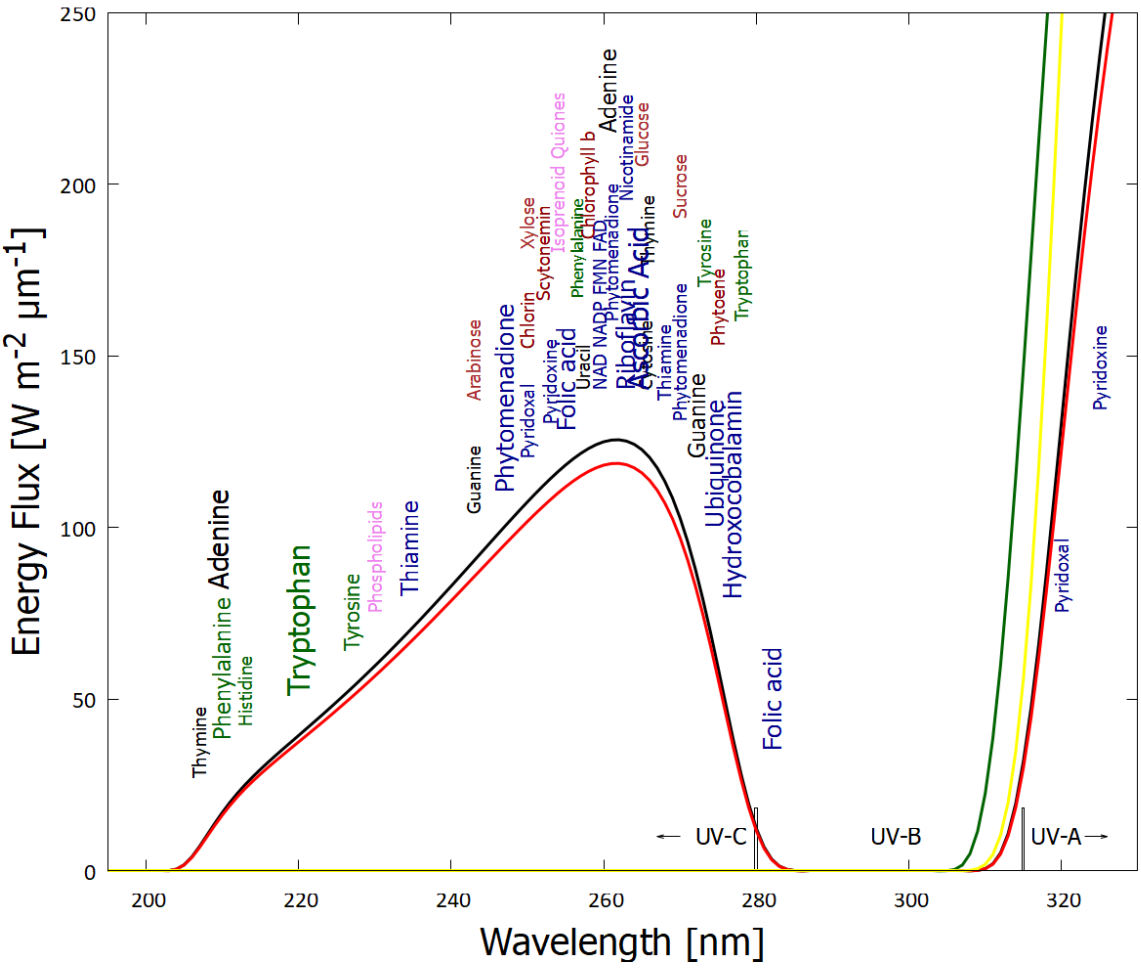

Figure 1.2: Light spectrum present at Earth's surface at different ages. The black line corresponds to 3.85 Ga (1 Ga = 10^9 years; it means a giga-year), the red to 2.9, the yellow to 2.2, and the green to the present. The black and red lines correspond to ages before the origin of life. Shielding below $\sim$ 205 nm is due to CO_2 and some H_2S in the atmosphere. Similarly, the presence of atmospheric aldehydes reduces the intensity of the spectrum between 285 and 310 nm [2]. About 2.2 Ga (yellow line), the intensity of UV-C photons was reduced by the increase of oxygen and ozone produced by live organisms performing oxygenic photosynthesis. Energy fluxes correspond to the sun at the zenith. The names covering the red and black spectrum correspond to the fundamental molecules of life plotted at their maximum absorption wavelength, and their font size is proportional to their respective molar extinction coefficients. Their color follows this code: nucleic acids (black), amino acids (green), fatty acids (violet), sugars (brown), vitamins, co-enzymes, co-factors (blue), and pigments (red). The name labels approach the energy flux curve in the UV-C region. Adapted from [3].

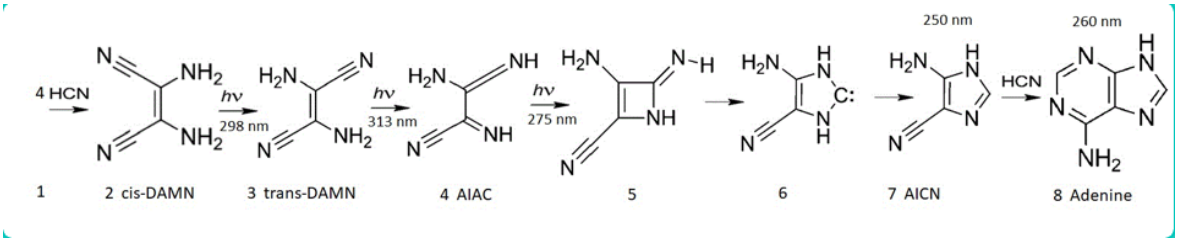

Figure 1.3: A possible adenine synthesize route based on chemical and photochemical reactions. Here are shown the main steps in the formation of adenine from HCN precursor. The process involves the absorption of several photons in the UV-C region. The final step, the adenine molecule, has a conical intersection that allows the systems to rapidly (sub-picoseconds) transform the photon energy into heat. Therefore, the adenine allows for efficient photon dissipation and is chemically stable because there is insufficient time to further chemical reactions. Adapted from [1].

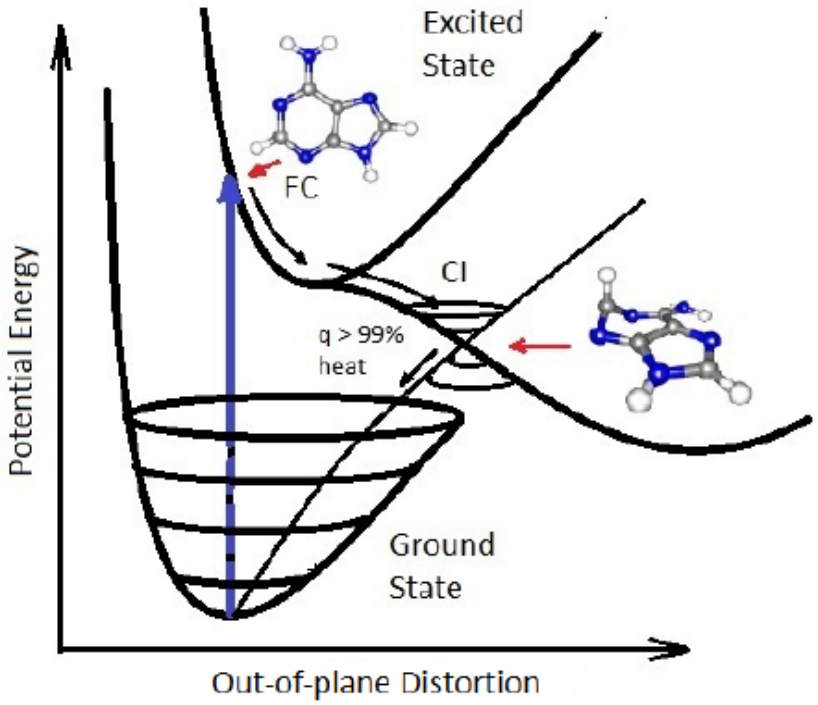

Figure 1.4: Conical intersection of adenine. Here, the degeneracy of the electronic excited and ground states can be seen. A photon absorption induces a geometry change known as pyrimidilization (a nuclear coordinate deformation) from its original structure in the Franck-Codon (FC) region. The deformed state allows the existence of a region CI where the vibrational states of the excited state coincide with the vibrational states on the ground state. The quantum efficiency of the dissipation of the original excitation into heat is almost 100%; this property provides photochemical stability to the molecule and makes the adenine very efficient for photon dissipation. Adapted from [1].

1.2 Prebiotic vesicles or protocells

At some time in the Earth's history, life became cellular. The primary function conferred to the cellular form is compartmentalization. The acquisition of boundaries has several advantages for a chemical system [27]. With a barrier, the reactants concentrate inside the system and separate from the medium. The increase in concentration induces a catalytic effect for further chemical reactions. Energy and matter can be exchanged through the barrier. The barrier provides selective permeability. Permeability allows nutrients to come into and the waste to be expelled. The barrier allows for gradients that can be useful for energy supply. The compartmentalization of chemical systems allows them to be differentiated from each other, each with their proper composition.

Modern cells have cell walls composed mainly of phospholipids, fatty acids, cholesterol, and phospholipid ethers. These molecules are amphiphilic and produce bilayers that assemble into vesicles by minimization of Gibbs's free energy. However, less complex molecules are expected to be the forebearers of cellular chemical systems, and some evidence indicates that the cellular ancestors were devoid of complex phospholipids [28, 29]. The more plausible molecules for protocell formation are long-chain fatty molecules, for example, fatty acids, long-chain alcohols, monoalkyl, and dialkyl phosphates [27]. Given ocean surface agitation, the formed vesicles could encapsulate the precursors of the fundamental molecules of life and other relevant compounds.

Forming life fundamental compounds requires a geochemical scenario with the following components: liquid water, an energy source (either geothermal or UV radiation),

minerals, and organic carbon precursors [27]. Hydrothermal vents are possible scenarios that have the previous requisites [30]. However, from TDTOEL's perspective, the most likely scenario for the origin of life is the ocean surface with UV-C radiation as the energy source, as discussed in section 1.1.

Conjugated fatty acids absorb strongly in the UV-C region, can be dissipatively structured through photo-chemical routes with UV-C photons, and have conical intersections [4]. Therefore, they have been proposed to be the likeliest amphiphilic molecules that could form protocells [4]. In addition, fatty acids are components of modern membranes of cells from all three domains of life [29], which suggests that fatty acids were essential in the earliest stages of life.

1.3 Dissipative structuring of conjugated fatty acids

The basic structure of fatty acids is a carboxyl head group with a hydrocarbon tail of 4 to 40 carbon atoms [31]. Simple fatty acids can be formed by polymerizing small chains of ethylene C_2H_4 through Fischer-Tropsch synthesis reaction or soft UV-C photochemical polymerization of UV-C light [4]. Ethylene comes from reducing CO_2 or CO in water or UV methane photolysis [4].

Vesicles formed with 18 carbons fatty acids have stability at high temperatures $\sim$85°C, (85°C is the Earth's average surface temperature as obtained from isotopic evidence in sediments dating back to the origin of life [32, 33]). The critical vesicle concentration (CVC) of fatty acids vesicles decreases with the increase of the alkyl chain length (the longer chains promote the packing of bilayers). The triple conjugated form of fatty acids absorbs strongly at about 260 nm [4]. The Archean fossil record shows that 16 and 18 carbons fatty acids were predominant [34,35]. The dominant presence of even numered carbon fatty acids can be explained if the fatty acids were formed through the polymerization of ethylene. The polymerization of ethylene starting from CO or CO_2 saturated water has been described previously [4, 36]. The melting temperature of vesicles usually increases as the carbon tail of the fatty acids length increases. If the degree of hydrogen saturation increases, the melting temperature of the vesicle

will increase. The increase in the melting temperature depends more significantly on saturation. Therefore, partially saturated and conjugated long-chain fatty acids could form stable vesicles under Archean high temperatures.

Previous work has shown that the formation of fatty acids was most likely through UV-C photochemical routes [4, 22, 37]. In these routes, the dissipative structuring process occurs in CO_2 saturated water at the ocean surface, forming ethylene and its polymerizations [4, 22]. Ethylene's polymerization rate is two orders of magnitude greater at 254 nm than 365 nm; note that the first wavelength belongs to the UV-C region and the second to the UV-A region.

Another possible photochemical route to fatty acids formation begins with formaldehyde under UV-C and UV-B radiation and with ZnO and TiO_2 acting as photocatalysts. The reaction products are 2 to 5 carbons fatty acids and other fundamental molecules of life [38]. The process includes the oligomerization of HCN into diaminomaleonitrile DAMN; this transformation can be induced by the absorption of photons in the region of 205 to 285 nm. A similar process occurs during the dissipative structuring of the purines [15, 24].

From the dissipative perspective, conjugated fatty acids are more relevant for the origin of life than saturated ones. The saturated fatty acids have negligible absorption in the UV-C region, except for absorption below about 180 nm, which induces dissociation, and for carboxyl head group absorption at 207 nm [39]. In contrast, conjugated fatty acids have strong UV-C light absorption; for example, diene has two double bonds and absorbs strongly at 233 nm, triene with three double bonds absorbs at 269 nm, and tetraene with four double bonds absorbs between 310 and 340 nm. In addition, conjugated fatty acids have conical intersections [40], giving them a high efficiency for dissipating photons into heat. Moreover, the conjugation of fatty acids can be achieved by a photochemical route using light between 205 and 285 nm in the UV-C region. This light can induce deprotonation, leading to the conjugation of carbon bonds in the acyl tail [41]. The fatty acids reach the conjugated form after several deprotonation events and migration of the double bonds [4].

The cross-linking between fatty acids adjacent tails at the locations of the double

bonds reduces the average conjugation number [42]. UV-C photons can induce cross-linking. Under the constant flux of UV-C light, a stationary state distribution of the conjugation number of the fatty acids would arise [4], and, given the incident light spectrum, the maximum conjugation number would be a triple conjugation which has an absorption at 269 nm.

The photochemical route to fatty acids formation can be summarized in the following steps [4]; i) UV-C-induced reduction of CO_2 or CO in water saturated with these, forming ethylene, ii) UV-C-induced polymerization of ethylene to form long hydrocarbon tails of an even number of carbon atoms (e.g., 18C), iii) oxidation and hydrolysis events to stop the growth of the chain and form the carboxyl head group, respectively, iv) UV-C induced deprotonation of the tails to form double carbon-carbon bonds, v) double bond migration to give a conjugated diene, triene, or tetraene molecule with a conical intersection. This process is represented in figure 1.5.

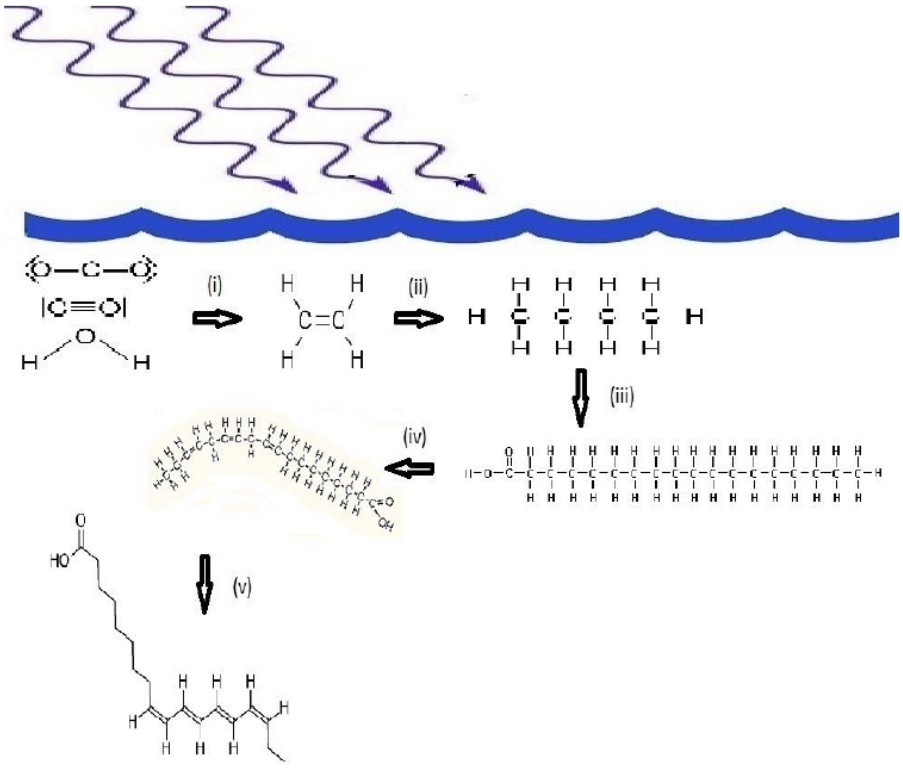

Figure 1.5: Dissipative structuring of fatty acids through a UV-C light photochemical route. More details are in section 1.3. Adapted from [4].

As an example, there is the fully conjugated linolenic acid which possesses the properties discussed above. It has a strong and wide absorption at 269 nm, and the vesicles formed with these fatty acids have a melting temperature of 85°.

1.4 Fatty acids vesicle formation

After forming the fatty acids, different structures can be formed spontaneously by minimizing Gibbs's free energy due to fatty acids amphiphilic nature [43]. The phase transitions between these structures have been addressed broadly in previous work as a function of temperature, solution's pH, reactants concentration, and chemical additives [44–48]. Vesicles are considered to be precursors of protocells.

The formation and stability of fatty acid vesicles have some inconveniences. 1) The narrow range of alkaline pH that allows the vesicle formation [49], 2) the salt flocculation (crystallization at high salt concentrations) [50,51], and, 3) the high critical vesiculation concentration (CVC critical value for spontaneous vesicle formation), it is even higher than the equivalent for phospholipids vesicles [52, 53].

The covalent cross-linking of neighboring chains of fatty acids can improve the pH stability and salt flocculation resistance of fatty acids vesicles. The covalent cross-linking could be induced by the following mechanism or any combination of them: UV-C light, temperatures above 50°C, and aging [42, 53]. If the fatty acid bilayer is formed with a structure consisting of a side-by-side overlap of the chains of each layer, with an overlap of the double bonds, then the vesicle has stability in a wider range of pH (2-14) [52]. This structure also promotes cross-linking by the three mentioned mechanisms. This structure is shown in figure 1.6.

Our general model of a fatty acids vesicle is shown in figure 1.7. The vesicle traps the precursor molecules involved in the dissipative structuring of the fundamental molecules of life, and the membrane allows for selective diffusion. The small precursor molecules can flow inside the vesicle, but the products, like adenine A, remain inside the vesicle.

The fatty acids membrane and the solution inside the vesicle constitute an optical system; see figure 2.1. Since we have suggested that the origin of life is highly related

to the interaction of matter with UV-C light, understanding how this optical system affects the light behavior and how it is related to the dissipative structuring of the fundamental molecules of life are relevant questions for the TDTOEL. The Mie theory for light scattering will be discussed in the next section; it is an important part of the thesis since the vesicles are modeled as Mie scattering particles.

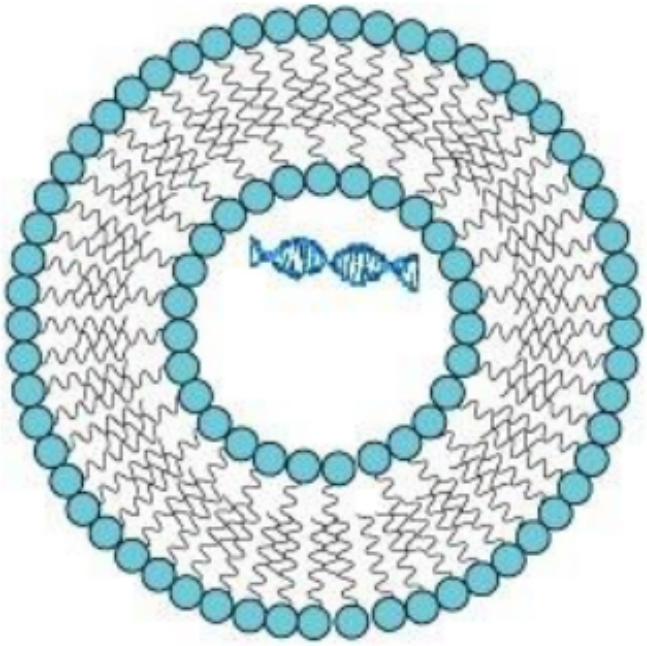

Figure 1.6: A fatty acids vesicle where the chains of each fatty acids layer are side-by-side overlapped. The overlap may occur at double bonds, facilitating cross-linking. Adapted from [4].

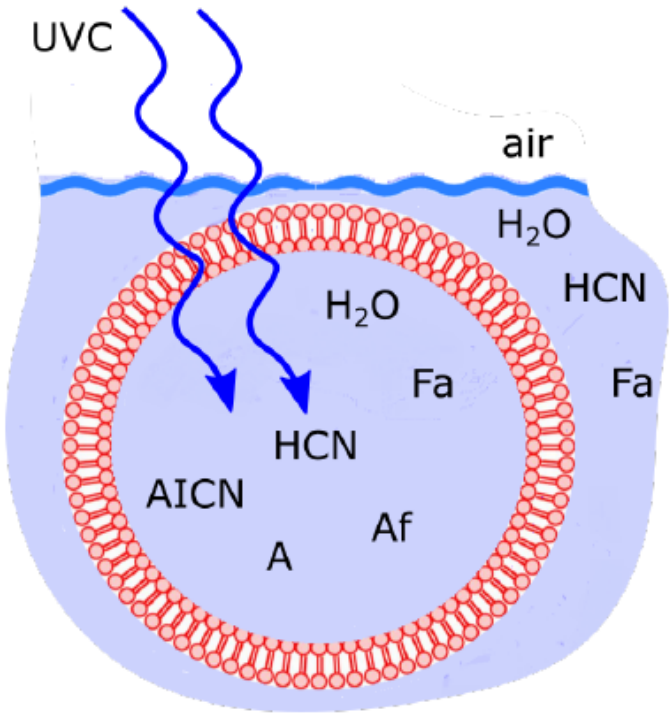

Figure 1.7: A fatty acids vesicle. The precursor molecules of the fundamental molecules of life are contained within it. A UV-C photon flux traverses the vesicle, allowing for dissipative structuring of the fundamental molecules of life. The precursor molecules can flow into the vesicle through the membrane by simple diffusion, but the products remain trapped inside the vesicle. Adapted from [4].

1.5 Mie scattering theory for a coated sphere

Once an electromagnetic wave impinges on a particle embedded in a medium, the particle's material polarizes. The polarization induces the formation of dipoles on the material, which then oscillate with the incoming wave and produce the scattered field. Additionally, some of the incoming radiation can be absorbed by the particle's material. A complex refractive index $\bar{n} = n + ik$ optically characterizes the particle with the real part related to the scattering and the imaginary part related to absorption.

To solve the problem of scattering and absorption by a small particle, consider a given particle embedded in a medium with specific size, shape, and optical properties illuminated with an arbitrarily polarized monochromatic wave. The solution consists in

finding the electromagnetic field at all points inside the particle and in the surrounding medium. We are considering only plane harmonic waves for simplicity, but since every arbitrary wave can be decomposed into its Fourier components, the solution can be generalized.

The electromagnetic fields inside the particle and in the medium can be decomposed into a component due to the incoming wave and a component due to scattering. The fields should satisfy Maxwell's equations.

If the surrounding medium is not absorbing, the electric power flowing through a spherical surface covering the particle (W_{abs}) can be divided into two terms, power due to scattering W_{sca} plus power due to extinction W_{ext} where $W_{ext} = W_{abs} + W_{sca}$. If I_i is the incident irradiance, the ratio of W_{ext} to I_i is called the extinction cross-section C_{ext} and has units of area. Thus, the absorption and scattering cross-sections are defined as $C_{abs} = \frac{W_{abs}}{I_i}$ and $C_{sca} = \frac{W_{sca}}{I_i}$. Finally, the efficiencies for extinction, scattering, and absorption are defined as $Q_{ext} = \frac{C_{ext}}{G}$, $Q_{sca} = \frac{C_{sca}}{G}$, $Q_{abs} = \frac{C_{abs}}{G}$. Where G is the geometrical cross-section of the particle ($G = \pi a^2$ for a sphere of radius a). The definitions show that "efficiency" does not refer to a quantity bounded by 1. Efficiencies should be interpreted as dimensionless cross-sections. Since photons are quantum waves interacting with the sphere's edge, the efficiencies can be greater than 1 and can show a diffraction-like partner.

With Mie's theory is possible to find solutions for Maxwell equations when the electromagnetic field is in a linear, isotropic, and within a homogeneous medium. For this case, we can use a generating function of vector harmonics ψ, which satisfies the scalar wave equation. For a spherical particle, ψ is chosen to satisfy the wave equation in spherical coordinates r, θ, ϕ and in separated variables $\psi(r, \theta, \phi) = R(r)\Theta(\theta)\Phi(\phi)$. The substitution of this solution into the scalar wave equation in spherical coordinates leaves three separate equations, one for each variable. We need linear independency in solutions to Φ, and ψ should be a single-valued function of ϕ. Θ should be finite at $\theta = 0, \pi$. It is known that the linearly independent solutions of Φ are $\phi_e = \cos m\phi$ and $\phi_o = \sin m\phi$, where e means even, o means odd, and m is a separation constant. The solutions of Θ corresponds to the associated Legendre functions, and the radial

solutions correspond to spherical Bessel functions. Finally, ψ is used to generate the electromagnetic vector. For further details on calculations refer to [54].

The electromagnetic vector (inside and outside the spherical particle) is expanded in vector spherical harmonics. For a given n in the expansion, two types of coefficients are relevant to our study. The scattering coefficients a_n and b_n (equations 1.3 and 1.4) are enough to calculate all quantities associated with scattering and absorption.

$$a_n = \frac{\mu m^2 j_n(mx)\left[x j_n(x)\right]' - \mu_1 j_n(x)\left[mx j_n(mx)\right]'}{\mu m^2 j_n(mx)\left[x h_n^{(1)}(x)\right]' - \mu_1 h_n^{(1)}(x)\left[mx j_n(mx)\right]'}, \tag{1.3}$$

$$b_n = \frac{\mu_1 j_n(mx)\left[x j_n(x)\right]' - \mu j_n(x)\left[mx j_n(mx)\right]'}{\mu_1 j_n(mx)\left[x h_n^{(1)}(x)\right]' - \mu h_n^{(1)}(x)\left[mx j_n(mx)\right]'}, \tag{1.4}$$

where $\mu = \cos(\theta)$, j_n are the spherical Bessel function, $x = \frac{2\pi N a}{\lambda}$ is the size parameter (N is the real refractive index of the sphere), $m = \frac{N_1}{N}$ (N_1 is the refractive index of the medium), and $h_n^{(1)}$ are the spherical Hankel functions.

A coated sphere consists of a sphere of radius a concentric with another sphere of radius b where $b > a$. The space between the spheres is called the mantle, and the space covered by the small sphere is called the core. If the scattering particle is a coated sphere, we should consider the electromagnetic field divided into three regions: the core, the mantle, and the surrounding medium. Although the procedure to solve this problem is similar to the one described above since the scattering and absorption depend on the particle's optical properties (now we have optical properties depending on space coordinates), the solution change. However, it is still possible to find analytic solutions for the scattering coefficients.

For further details on Mie's theory for scattering and absorption by small particles, the reader is referred to reference [54].

Chapter 2

Simulation of a fatty acids vesicle

2.1 Model

The fatty acids vesicles or protocells are modeled as coated spheres embedded in the ocean surface. Incoming light from the sun arrives at the air-water interface; see figure 2.1. The core of the coated sphere consists of a water solution of fundamental molecules of life, mainly DNA, which is covered by a fatty acids bilayer. The fatty acids bilayer is labeled as the mantle of the coated sphere. Since the fatty acids constitute the vesicle's membrane, we shall also refer to the mantle as the membrane. The fatty acids are considered to have $\sim$18 carbons.

In addition to linolenic acid, the 12-phenyl dodecanoic acid is another plausible candidate to conform the fatty acids membrane. It also has 18 carbon atoms. The overlapped bilayer structure is formed by overlapping the aromatic rings of the fatty acids of the two layers.

The incoming light goes into the water and interacts with the vesicle. The light can be scattered in all directions or absorbed by the fatty acids or the core solution. The scattering of light can change the polarization of the incoming unpolarized light to linear polarization. Total internal reflection of the scattered light at the air-water interface may occur, producing a circular polarization component; see figure 2.1. Depending on the direction of observation, the beam is either left or right-handed circularly polarized [5].

Due to the absence of published data on the UV-C absorption spectrum of these two fatty acids, we approximated the absorption of the 12-phenyl dodecanoic acid by the absorption of the cinnamic acid [10]. Both fatty acids are very similar; their carbon chain length is the only difference. However, the error induced by using any fatty acid absorption spectra would not be large since the vesicle wall (the mantle) is very small compared with the vesicle size. Thus the membrane contributes little to absorption and scattering.

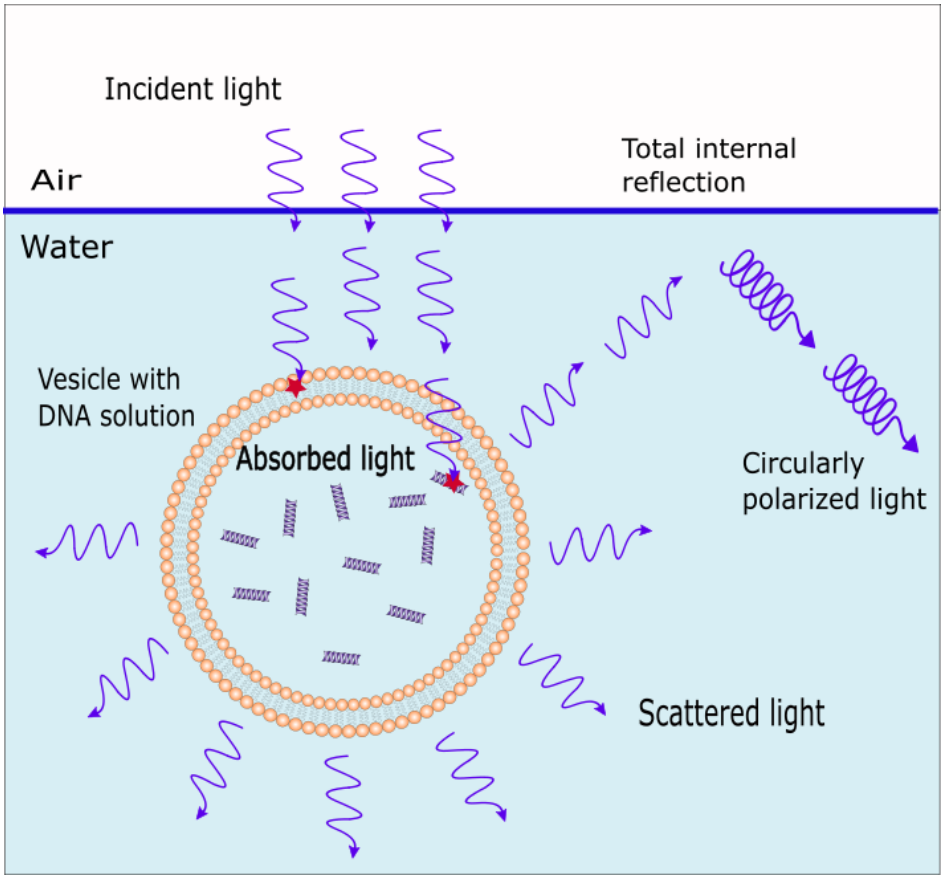

Figure 2.1: UV-C light interacting with a fatty acids vesicle. Incoming UV light from the sun travels through the air-water interface and interacts with the vesicle. Part of the light is scattered in all directions, and another part is absorbed by the membrane or the DNA solution inside the vesicle. Part of the light scattered in the backward direction can be totally internally reflected at the air-water interface producing circularly polarized light. The circularly polarized light could promote the acquisition of homochirality by DNA [5].

The optical properties of the vesicle were established as follows: first, the real

refractive index n of water was taken from published data [6]. In the case of DNA, RNA, and the other fundamental molecules of life in water solution inside the core, the real refractive index depends on the concentration; for example, Figure 5 in reference [55] shows that the index of refraction is an increasing function of DNA concentration in water solution. The real refractive index of the vesicle core was obtained from experiments by Liu et al. [56]. They show that n for modern-day cell nuclei lies between 1.353 and 1.367, corresponding to a scale factor of 1.01 and 1.02 times that of pure water at 589 nm (n=1.34). Due to the absence of published data of n as a function of wavelength for the core solution, we took it to be the same as pure water multiplied by the corresponding scale factor. For fatty acids, we also consider the wavelength dependence of n to be the same as pure water but anchored to 1.39 at 589 nm, which is the value of n for cinnamic acid at that wavelength [7]. See figure 2.2.

The extinction coefficient k (imaginary part of refractive index) for water was taken from [6, 8]. k for the fundamental molecules in water solution depends on the molar extinction coefficient ϵ, and on the concentration c of the DNA in water. ϵ for the DNA water solution was obtained from [9]. The explicit dependence of k is $k(\lambda) = \frac{\lambda}{4\pi}\epsilon \cdot c$. We used c as a multiplicative factor to make scattering and absorption results noticeable. Note that it is the ratio of scattering and the ratio of absorption in the different wavelength regions, not the absolute values of these, which is important to the results. k in the function of wavelength for the fatty acids membrane was taken from cinnamic acid data [10]. See figure 2.3. In this model, we are approximating the optical properties of the 12-phenyl-dodecanoic with the data of cinnamic acid (both fatty acids are aromatic, the only difference is the length of their hydrocarbon tail).

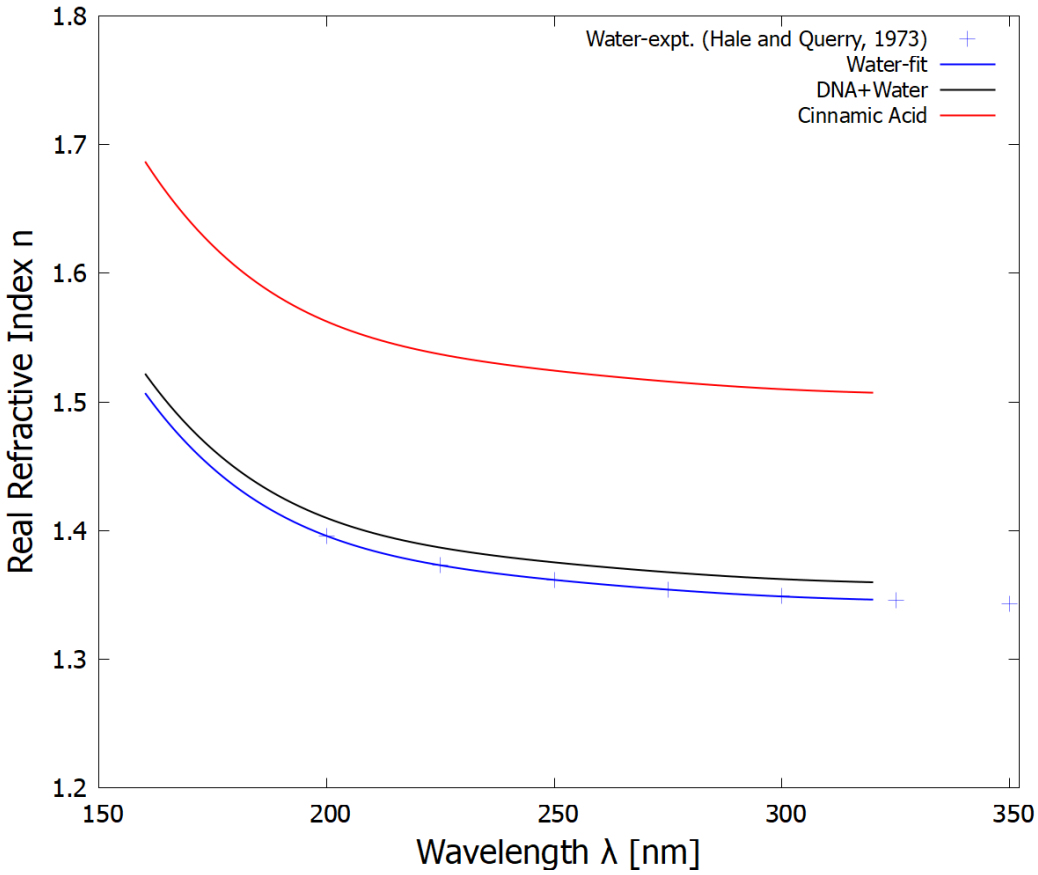

Figure 2.2: Real refractive index n for each component of the vesicle model. n for water is in blue, n for the solution of DNA, RNA, and other fundamental molecules in water solution is in black, and n for the fatty acids membrane is in red. Blue crosses are the experimental data for water obtained from [6]. The black line was taken to be the refractive index of water multiplied by the factor 1.01 (see section 2.1). n for fatty acids was anchored to 1.39 at 569 nm, which is the value measured for cinnamic acid ($C_9H_8O_2$) [7] (which should be similar to 12-phenyl-dodecanoic acid since both have aromatic geometry) and was given the same wavelength dependence as that of water. However, due to the small thickness of the mantle (5 nm) compared with the vesicle core, any change in its n values does not have a noticeable effect on scattering and absorption.

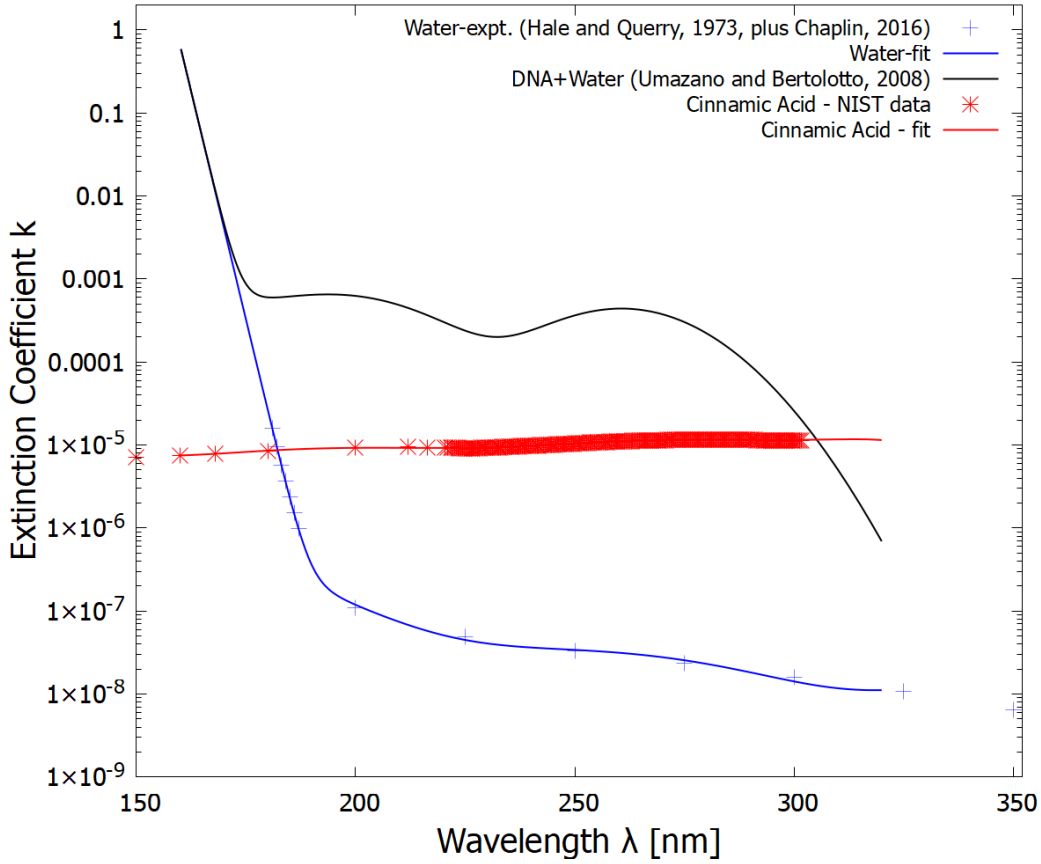

Figure 2.3: Imaginary part of the refractive indexes k of the components of the vesicle model. The blue line corresponds to pure water; it is a fit to experimental data (blue crosses) [6, 8]. The black line is k for the DNA solution in water; it was obtained by multiplying the data from [9] by 10 (see section 2.1), which approximate k for the water solution of DNA, RNA, and other fundamental molecules of life within the vesicle. k for the fatty acids membrane is plotted as a red line, which is a fit to experimental data [10].

2.2 BHCOAT code for Mie Scattering

We use BHCOAT to simulate Mie scattering for our fatty acids vesicle model; see section 2.1. The BHCOAT code [54] calculates the extinction efficiency, Q_{ext}, the scattering efficiency, Q_{sca}, the absorption efficiency, Q_{abs}, and the backscattering efficiency, Q_{back}, for a coated sphere for unpolarized light. The simulation is based on Mie's theory, valid when the vesicle size is larger than the incident wavelength.

The BHCOAT inputs are the incident light wavelength, the radius of the vesicle

core, the thickness of the fatty acid membrane (estimated to be 5 nm for a bilayer of 18-carbon atom fatty acids), the real refractive index of the surrounding water medium, and the complex refractive indexes of the fatty acids membrane and the core solution of DNA, RNA and other fundamental molecules in water solution. These quantities are either independent variables or are described in section 2.1.

Chapter 3

Results

3.1 Scattering and Absorption

The efficiencies Q_{ext}, Q_{sca} and $Q_{abs} = (Q_{ext} - Q_{sca})$ (see section 1.5) were integrated over the wavelength regions of 245-275 nm (soft UV-C region) and 180-210 nm (hard UV-C region).

For the case of the vesicle core having a real refractive index of that of pure water multiplied by 1.01, the graphs of the integrals are shown in figure 3.1. The 1.01 factor for water corresponds to the lowest real refractive index of today's cells. An expected diffraction pattern appears for small radii. Some radii show a photo-protective effect against the hard UV-C light when Q_{sca} is maximum for the integrated region of 180-210 nm (blue curve, figure 3.1); these radii of maximum hard UV-C scattering are 4.4 and 11.8 μm. The energy in these hard UV-C wavelengths is sufficient to dissociate nucleic acids, amino acids, proteins, and other fundamental molecules of life trapped inside the vesicle. The photo-protective effect of Mie scattering would reduce the disassociation of the fundamental molecules, allowing the fundamental molecules to be more efficient at absorbing and dissipating in the soft UV-C (245-275 nm) region (figure 1.2). Note that the soft UV-C light is considerably more scattered than absorbed when the core radius is small.

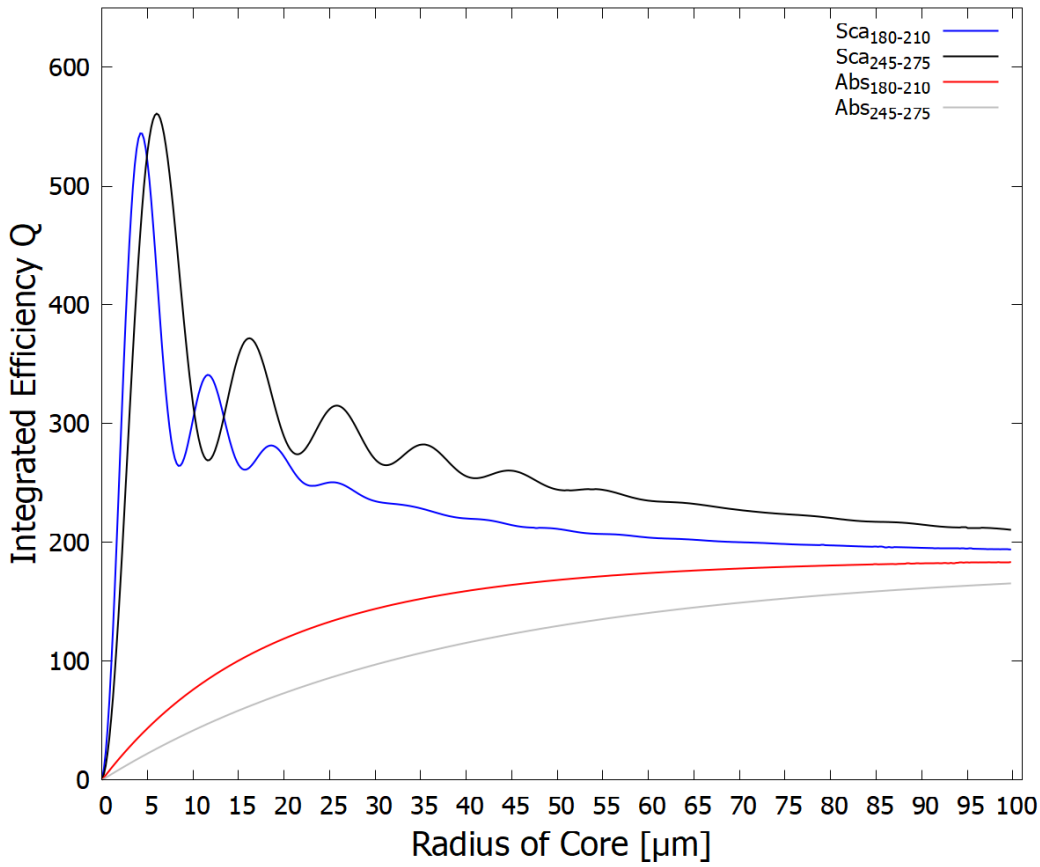

Figure 3.1: Graphs of the integrated efficiencies of scattering Q_{sca} and absorption Q_{abs} presented to the light beam of the fatty acid vesicle. The integrals covered two different wavelength regions (180-210 nm - ionizing/disassociation region - Hard UV-C region) and (245-275 nm - dissipative structuring region - Soft UV-C region) as a function of the vesicle core radius. In this simulation, the real refractive index of the vesicle core was taken to be that of pure water multiplied by the factor 1.01; see figure 2.2. The blue line corresponds to integrated scattering efficiency in the hard UV-C region. The maxima of the blue line are the vesicle radii that provide more hard UV-C shielding to the core and are located at about 4.4 μm with a smaller peak at 11.8 μm, which would correspond to vesicles of a diameter of about 8.8 and 23.6 μm respectively (consider that the membrane width is 5 nm).

The results using a real refractive index for the vesicle core that of pure water multiplied by the second factor of 1.02 are shown in figure 3.2. Note that if the real refractive index of the core increases, then the maximum of hard UV-C wavelengths integrated scattering moves to smaller radii (blue line). In this case, the maxima are located at 2.2 μm with a lesser peak at 5.9 μm, corresponding to vesicle diameters[1] of

[1]Since the vesicle is been modeled as a layered sphere, the radius of the sphere corresponds to

4.4 and 11.8 μm, respectively.

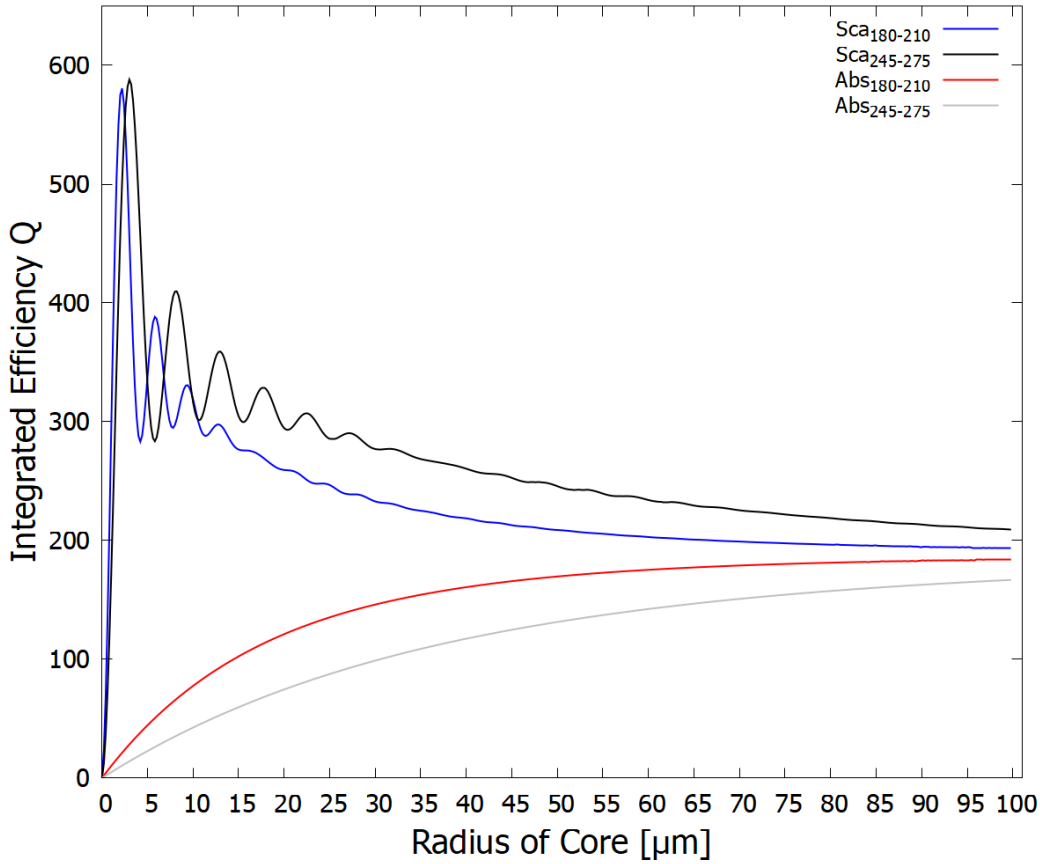

Figure 3.2: The same quantities as in figure 3.1 but the real reactive index of the vesicle core is that of pure water multiplied by 1.02 instead of 1.01. The color code is the same than in figure 3.1. The greatest shielding against ionizing radiation (blue line) occurs at a smaller vesicle core radius of about 2.2 μm with a smaller peak at 5.9 μm, corresponding to vesicle diameters of about 4.4 and 11.8 μm respectively.

The extinction, scattering, and absorption efficiencies as a function of wavelength are plotted for different vesicle sizes in figures 3.3 and 3.4. The results in figure 3.3 correspond to vesicle radii of 4.4 (solid lines) and 11.8 μm (dashed lines). At these radii values, the integrated scattering in the hard UV-C region (ionization/disassociation region, 180-210 nm) is maximum; see figure 3.1. The maximum integrated scattering efficiency in the hard UV-C region provides photoprotection to the interior of the vesicle

half of the diameter of the vesicle. The membrane increases the vesicle diameter with 10 nm which is negligible.

against harmful photons. For the smaller vesicle of 4.4 μm core radius, the scattering in the hard UV-C is about 2.8 times greater than that expected classically, given the geometrical cross-section.

Small vesicle radii could help shield these molecules of life when there was lower CO_2 or little H_2S (ejected from volcanoes) in the atmosphere. However, since scattering in the soft UV-C region is also quite strong, absorption (solid red line, figure 3.3) in the soft UV-C region is quite small.

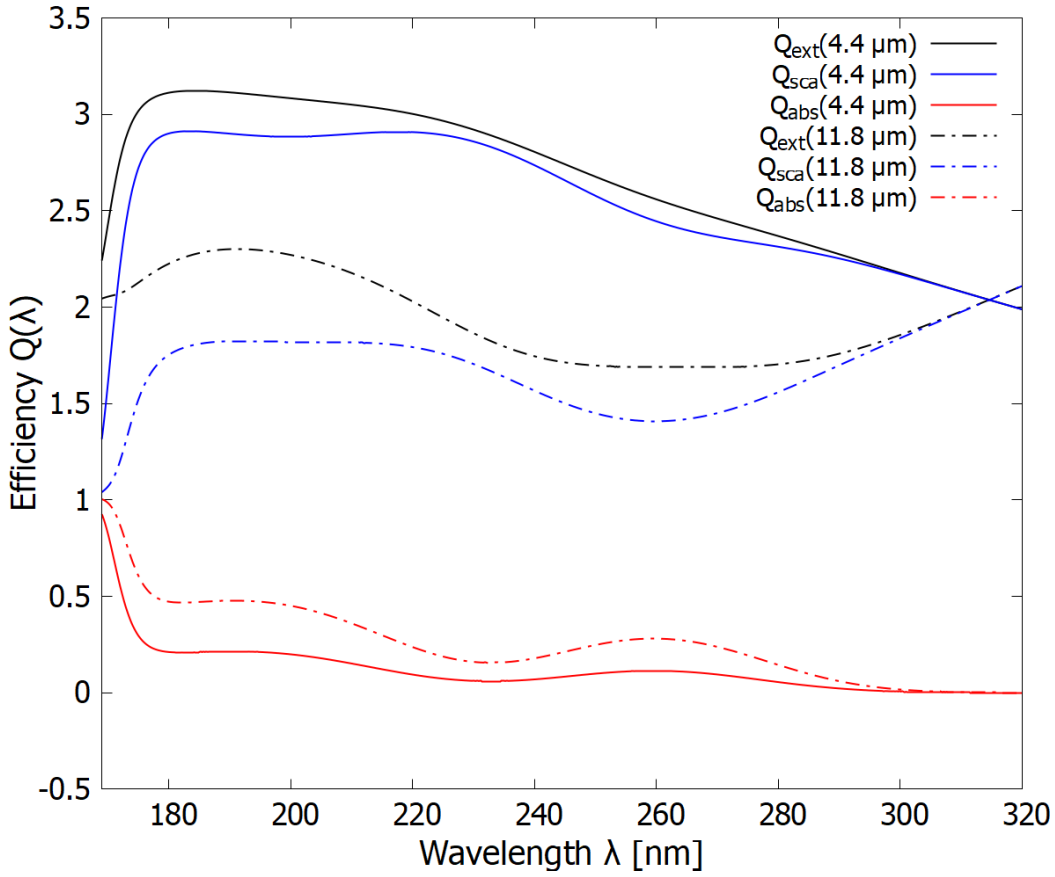

Figure 3.3: Plotts of extinction, scattering, and absorption efficiencies (ratio of the observed cross-section to the geometrical cross-section of the vesicle) as a function of wavelength for two vesicle radii, 4.4 μm (solid lines) and 11.8 μm (dashed lines). The greater scattering (photo-protective effect) is located in the hard UV-C region (180-210 nm). In the larger radius, the scattering decreases (dashed blue line) in the hard UV-C region, but absorption (red dashed line) in the soft UV-C (245-275 nm) region increases.

In figure 3.1, a second and smaller maximum of photo-protection (blue line) is lo-

cated at 11.8 μm of vesicle core radius. The efficiencies for scattering at this vesicle size are plotted in figure 3.3 (blue dashed line). At this radius, although the scattering of hard UV-C photons is smaller than when the radius is smaller, it is still significant. At the same time, more light is absorbed in the soft UV-C region, which is the dissipative structuring region.

The largest vesicle studied here has a core radius of 100 μm (figure 3.4). Here, the scattering and absorption in the hard UV-C region are almost equal, and a maximum for absorption in the soft UV-C region appears. Such vesicle radii would thus be relevant when there was more CO_2 or H_2S in the atmosphere to protect the vesicle from the hard UV-C light.

The larger vesicle sizes show less scattering in the hard UV-C region (ionization/dissociation region, see figure 3.4) but show greater absorption in the soft UV-C region (dissipative structuring region). On the other hand, vesicles of smaller sizes show a more significant photo-protective effect in the hard UV-C region but less absorption in the soft UV-C region (see figure 3.3).

The previous results may indicate a natural thermodynamic selection process of the vesicle size that could have occurred to optimize the dissipative structuring of the fundamental molecules of life under soft UV-C photons and to increase the probability of survival of the fundamental molecules under different environmental scenarios, primarily the survival under the presence of hard UV-C photons. The selection process could depend on the prevailing light conditions through the geological ages. Depending on atmospheric conditions, small vesicles could proliferate when hard UV-C photons arrived considerably to the Earth's surface and big vesicles could proliferate when less hard UV-C photons arrived to the Earth's surface. In both cases, the scattering and absorption of the vesicle optimize the vesicles' survival rate and the fundamental molecules' dissipative structuring process inside the vesicle.

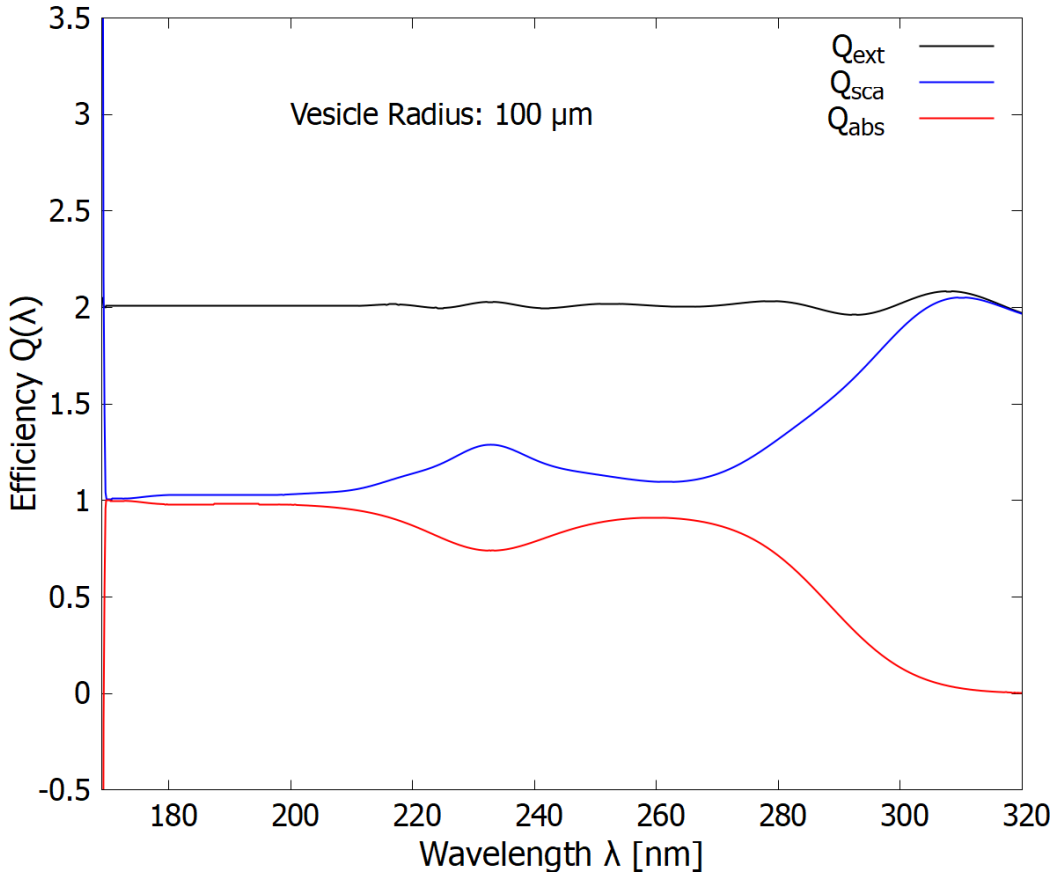

Figure 3.4: Plot of extinction, scattering, and absorption efficiencies (ratio of the observed cross-section to the geometrical cross-section of the vesicle) as a function of wavelength for a vesicle of radius 100 μm (this size corresponds to the larger bacteria of today). The photo-protective effect decreases in the hard UV-C region (180-210 nm). The decrease is considerable compared with smaller radii vesicles, see figure 3.3; instead, the absorption in the soft UV-C region (245-275 nm) increases considerably compared to the smaller radii vesicles, see figure 3.3.

In addition to the vesicle size, tuning the concentration of the fundamental molecules of life in solution inside the vesicle could also optimize the dissipative structuring under soft UV-C photons and increase the vesicle survival probability under hard UV-C photons. The optical properties of the vesicle depend on the solution concentration (compare figures 3.1 and 3.2), therefore, the optimization can be achieved by affecting the permeability of the vesicle. Adding a shorter chain, or conjugated (unsaturated and kinked), fatty acids to the vesicle wall is an example of changing the vesicle permeability.

3.2 Backscattering, Optical Dichroism, and Homochirality

The description of how the light scattered by the vesicle can produce circularly polarized light by total internal reflection of the scattered beams at the air-water interface is given in section 2.1 [5]. Previous results show that the ocean surface is, in fact, the region on Earth with the greatest presence of circularly polarized light, reaching up to 5% of the available submarine light at the ocean surface in the early morning or late afternoon [57].

Because fatty acids are not chiral molecules, they absorb similarly right and left-handed circularly polarized light; however, DNA and RNA are chiral molecules. From the given measured circular dichroism of the nucleic acids, the measured circularly polarized component of light today just beneath the ocean surface, and assuming a similar component during the Archean, and given the existence of ultraviolet and temperature-assisted denaturing of double-strand DNA or RNA [11], previous work showed that complete homochirality of DNA and RNA could have been produced in a few thousand Archean years [5].

The integrated backscattering (scattering in the backward direction) in the soft UV-C photons region (245-275 nm) as a function of vesicle radius is shown in figure 3.5. Backscattering increases with the vesicle radius as expected classically. The backscattered beams, along with some forward scattered beams at low solar angles, could be totally internally reflected at the ocean surface. The produced circularly polarized light could have contributed to the acquisition of homochirality through UV-C and temperature assisted denaturing [11] in the nucleic acids inside the neighboring vesicles.

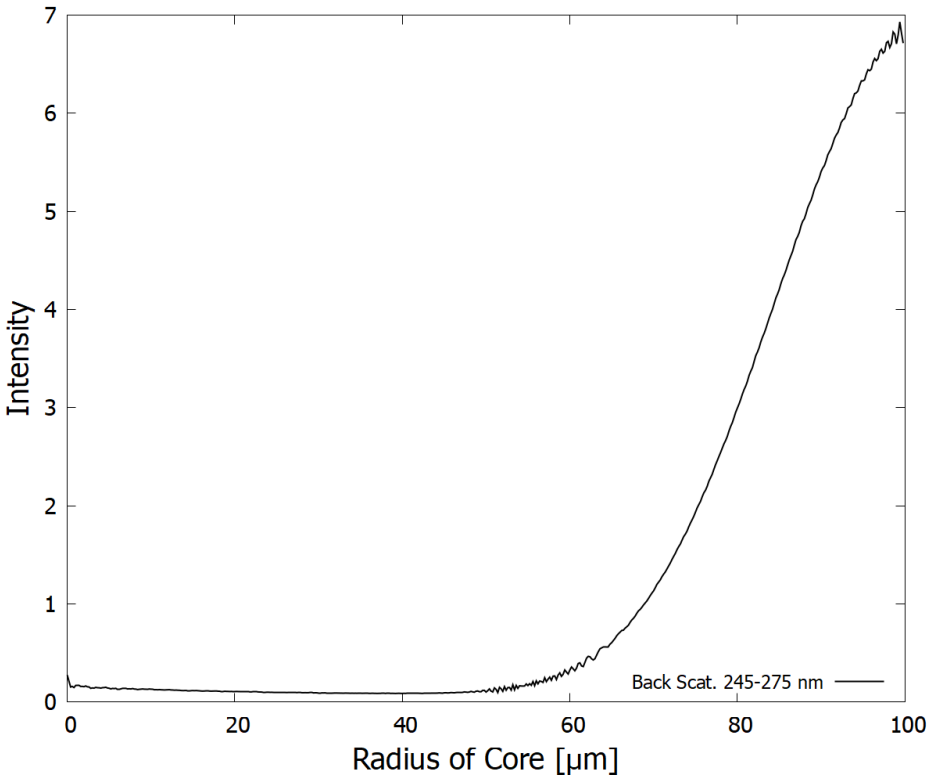

Figure 3.5: Integrated backscattering (scattering in backward direction) in the soft UV-C region (245-275 nm) as a function of vesicle core radius. The fatty acid membrane has a thickness of 5 nm, and the real refractive index of the core was taken as that of pure water multiplied by 1.01. The backscattering is an order of magnitude smaller than forward scattering and is relatively independent of the incident angle. The backscattering increases as the vesicle core radius increases. The backscattered light, in addition to some forward scattered beams at low solar angles, could be totally internally reflected at the air-water interface and would provide circularly polarized light helpful for the acquisition of homochirality by the nucleic acids trapped within the surrounding vesicles [5, 11]

Chapter 4

Conclusions

The Archean UV-C solar light flux's free energy promoted the structuring of life's fundamental molecules from precursor molecules like HCN and cyanogen on the ocean surface. Fatty acids were also dissipatively structured and performed the basic thermodynamic function of dissipating the incoming UV-C light into heat. The evidence includes the strong absorption of fatty acids in the UV-C region, their synthesis through photochemical routes operating in the UV-C region, and the fact that conjugated fatty acids have a conical intersection that provides them chemical stability and, more importantly, high photon dissipation efficiency. Fatty acids protocells or prebiotic vesicles could form under early-life Earth conditions.

This thesis, along with a simultaneous article [58], are the first studies known by the authors that address the optical properties of prebiotic vesicles in the UV-C region and that relate them with photon dissipation and the origin of life. Our model consists of a vesicle constituted of a fatty acid membrane that confines DNA and other fundamental molecules of life in water solution. The vesicle is embedded in the ocean surface. Sunlight is scattered and absorbed by the vesicle; part of the scattered light can be totally internally reflected at the ocean surface, producing circularly polarized light that could induce homochirality in the DNA and RNA of neighboring vesicles.

In our model, the real refractive index of the core was taken to be that of purified water multiplied by a factor of either 1.01 or 1.02, which spans the range of real refractive indexes at 569 nm found in current living cells. Improvement of the esti-

mations for the wavelength dependence of the real refractive index of the core in the UV-C region can be achieved by Kramers-Kroning relations once precise extinction coefficient measurements as a function of wavelength is given by future experimental measurements.

Mie scattering produced by this system could provide the fundamental molecules within the vesicle with a photo-protective effect against the hard UV-C photons present in the early atmosphere. The hard UV-C photons can ionize and dissociate, destroying the vesicle's fundamental molecules. We found that the maxima of scattering of the hard UV-C photons depend on the vesicle's core radius. The vesicle's maximum scattering of hard UV-C photons occurs at small vesicles (< 24 μm) when the concentration of fundamental molecules in the vesicle core is similar to that of modern bacteria having a real refractive index of 1.01 times that of pure water. Under the same conditions, the maximum absorption of soft UV-C photons occurs at vesicle sizes greater than 100 μm. Therefore, the core radius provides the vesicle with different optical properties in the UV-C region.

The radii of maximum scattering were found to be dependent on the concentration of the DNA and other fundamental molecules in water solution inside the vesicle core because the real refractive index of the core is a function of the core solution concentration. The vesicle sizes found at these maxima hard UV-C scattering regimes, given a concentration of the core solution similar to that of today's cells, are consistent with the dimensions of fossil bacteria discovered in sediments of the early Archean period [59] when intense UV-C light was arriving at Earth's surface. Figures 3.1 and 3.2 show that the radius of the vesicle at which a maximum of scattering is found is smaller as the real refractive index of the core increases.

The membrane of the vesicle contributes little to the scattering and absorption of the vesicle because the membrane has a small size (5 nm) compared to the core (> 1 μm). The primary function of the fatty acids membrane is to provide a container for the fundamental molecules and separate the systems into two parts: the ocean water outside the vesicle, and the fundamental molecules in water solution inside the vesicle, each with homogeneous optical properties.

Regarding thermodynamic selection, it is possible that vesicle sizes that promote dissipative structuring and increase the survival probability of the fundamental molecules could be selected over the others. The implications are different depending on the atmospheric composition at different Earth ages. For example, if the atmosphere were rich in CO_2 and H_2S, gases that absorb the hard UV-C photons, then a large vesicle size that gives greater soft UV-C photons absorption but less hard UV-C photon scattering could be selected. In fact, vesicles of independent (unicellular) bacteria have been found in Archean deposits with sizes of less than 24 μm at $\sim$ 3.43 Ga, while with dimensions of up to 289 μm at $\sim$ 3.2 Ga [59].

Fatty acid vesicles could have protected the fundamental molecules of life confined inside them from the dangerous hard UV-C radiation present at the origin of life, preventing dissociation through ionization. These properties could have important implications in finding life in any planetary system of different star types with a significant presence of UV-C light. A planet that does not have enough atmospheric CO_2 or hydrogen sulfide during a given epoch to avoid ionizing UV-C radiation on its surface could still support the dissipative structuring of life because of the presence of fatty acids vesicles. Therefore, the presence of fatty acids vesicles could increase the likelihood of finding carbon-based life on more planets than previously thought.

Bibliography

[1] Karo Michaelian. Non-equilibrium thermodynamic foundations of the origin of life. *Foundations*, 2(1):308–337, 2022.

[2] C. Sagan. Ultraviolet Selection Pressure on the Earliest Organisms. *J. Theor. Biol.*, 39:195–200, 1973.

[3] K. Michaelian and A. Simeonov. Fundamental molecules of life are pigments which arose and co-evolved as a response to the thermodynamic imperative of dissipating the prevailing solar spectrum. *Biogeosciences*, 12:4913–4937, 2015.

[4] K. Michaelian and O. Rodriguez. Prebiotic fatty acid vesicles through photochemical dissipative structuring. *Revista Cubana de Química*, 31(3):354–370, 2019.

[5] Karo Michaelian. Homochirality through photon-induced denaturing of rna/dna at the origin of life. *Life*, 8(2), 2018.

[6] George M. Hale and Marvin R. Querry. Optical constants of water in the 200-nm to 200-μm wavelength region. *Appl. Opt.*, 12(3):555–563, Mar 1973.

[7] C. Gardiner, M. Shaw, P. Hole, J. Smith, D. Tannetta, C. W. Redman, and I. L. Sargent. Measurement of refractive index by nanoparticle tracking analysis reveals heterogeneity in extracellular vesicles. *Journal of extracellular vesicles*, 3:25361, 2014.

[8] M. Chaplin. Water structure and science. 2016.

[9] J.P. Umazano and J.A. Bertolotto. Optical properties of dna in aqueous solution. *J Biol Phys.*, 34(1-2):163–177, 2008.

[10] Victor Talrose, Alexander N. Yermakov, Alexy A. Usov, Antonina A. Goncharova, Axlexander N. Leskin, Natalia A. Messineva, Natalia V. Trusova, and Margarita V. Efimkina. *NIST Chemistry WebBook*, chapter UV/Visible Spectra, in NIST Standard Reference Database Number 69. National Institute of Standards and Technology, Gaithersburg MD, 2023.

[11] K. Michaelian and N. Santillan. Uvc photon-induced denaturing of dna: A possible dissipative route to archean enzyme-less replication. *Heliyon*, 5:e01902, 2019.

[12] K. Michaelian. Thermodynamic origin of life. *ArXiv*, 2009.

[13] K. Michaelian. Thermodynamic dissipation theory for the origin of life. *Earth Syst. Dynam.*, 224:37–51, 2011.

[14] Karo Michaelian. *Thermodynamic Dissipation Theory of the Origina and Evolution of Life: Salient characteristics of RNA and DNA and other fundamental molecules suggest an origin of life driven by UV-C light.* Self-published. Printed by CreateSpace. Mexico City. ISBN:9781541317482., 2016.

[15] Karo Michaelian. The dissipative photochemical origin of life: Uvc abiogenesis of adenine. *Entropy*, 23(2), 2021.

[16] Karo Michaelian and Ramón Eduardo Cano. A photon force and flow for dissipative structuring: Application to pigments, plants and ecosystems. *Entropy*, 24(1):76, Jan 2022.

[17] D.W. Deamer. The role of lipid membranes in life's origin. *Life*, 7:5, 2017.

[18] I. Prigogine. *Introduction to Thermodynamics Of Irreversible Processes.* John Wiley & Sons, third edition, 1967.

[19] Paul Manneville. *Dissipative Structures and Weak Turbulence.* Academic Press, 1990.

[20] K. Michaelian. The biosphere. chapter The biosphere: A thermodynamic imperative, pages 51–60. INTECH, London, 2012.

[21] K. Michaelian. Biological catalysis of the hydrological cycle: lifes thermodynamic function. *Hydrol. Earth Syst. Sci.*, 16:2629–2645, 2012.

[22] K. Michaelian. Microscopic dissipative structuring and proliferation at the origin of life. *Heliyon*, 3:e00424, 2017.

[23] K. Michaelian. Photochemical dissipative structuring of the fundamental molecules of life. *Proceedings, 5th International Electronic Conference on Entropy and Its Applications; Session: Biological Systems*, 2019.

[24] Claudeth Hernández and Karo Michaelian. Dissipative photochemical abiogenesis of the purines. *Entropy*, 24(8):1027, Jul 2022.

[25] Hyuk Kang, Kang Taek Lee, Boyong Jung, Yeon Jae Ko, and Seong Keun Kim. Intrinsic lifetimes of the excited state of dna and rna bases. *Journal of the American Chemical Society*, 124(44):12958–12959, 2002.

[26] K. Michaelian. Thermodynamic stability of ecosystems. *Journal of Theoretical Biology*, 237(3):323 – 335, 2005.

[27] Augustin Lopez and Michele Fiore. Investigating prebiotic protocells for a comprehensive understanding of the origins of life: A prebiotic systems chemistry perspective. *Life*, 9(2):49, Jun 2019.

[28] J. Pereto, P. Lopez-Garcia, and D. Moreira. Ancestral lipid biosynthesis and early membrane evolution. *Trends Biochem. Sci.*, 29:469–477, 2004.

[29] J. Lombard, P. López-García, and D. Moreira. The early evolution of lipid membranes and the three domains of life. *Nature Reviews, Microbiology*, 10:507–515, 2012.

[30] M. Colín-García. Hydrothermal vents and prebiotic chemistry: A review. *Bol. Soc. Geológica Mex.*, 68(3):599–620, 2016.

[31] D.W. Johnson. A synthesis of unsaturated very long chain fatty acids. *Chemistry and Physics of Lipids*, 56(1):65 – 71, 1990.

[32] L. P. Knauth and D. R. Lowe. High archean climatic temperature inferred from oxygen isotope geochemistry of cherts in the 3.5 ga swaziland group, south africa. *Geol. Soc. Am. Bull.*, 115:566–580, 2003.

[33] L. P. Knauth. Temperature and salinity history of the precambrian ocean: implications for the course of microbial evolution. *Paleogeography, Paleoclimatology, Paleoecology*, 219:53–69, 2005.

[34] Jerry Han and Melvin Calvin. Occurrence of fatty acids and aliphatic hydrocarbons in a 3.4 billion-year-old sediment. *Nature*, 224(5219):576–577, 1969.

[35] William Van Hoeven, JR Maxwell, and Melven Calvin. Fatty acids and hydrocarbons as evidence of life processes in ancient sediments and crude oils. *Geochimica et Cosmochimica Acta*, 33(7):877–881, 1969.

[36] S. Rossignol, L. Tinel, A. Bianco, and M. Passananti. Atmospheric photochemistry at a fatty acid–coated air-water interface. *Science*, 353:699–702, 2016.

[37] C. N. Bowman and C. J. Kloxin. Toward an enhanced understanding and implementation of photopolymerization reactions. *AIChE J.*, 54:2775–2795, 2008.

[38] L. Botta, B. M. Bizzarri, D. Piccinino, T. Fornaro, J. R. Brucato, and R. Saladino. Prebiotic synthesis of carboxylic acids, amino acids and nucleic acid bases from formamide under photochemical conditions. *Eur. Phys. J. Plus*, 132:317, 2017.

[39] A. Vicente, R. Antunes, D. Almeida, I. J. A. Franco, S. V. Hoffmann, N. J. Mason, S. Eden, D. Duflot, S. Canneaux, J. Delwiche, M.-J. Hubin-Franskin, and P. Limão-Vieira. Photoabsorption measurements and theoretical calculations of the electronic state spectroscopy of propionic, butyric, and valeric acids. *Phys. Chem. Chem. Phys.*, 11:5729–5741, 2009.

[40] P. Celani, M. Garavelli, S. Ottani, F. Bemardi, M. A. Robb, and M. Olivucci. Molecular “trigger” for radiationless deactivation of photoexcited conjugated hydrocarbons. *J. Am. Chem. Soc.*, 117:11584–11585, 1995.

[41] T. K. Mandal and S. N. Chatterjee. Ultraviolet- and sunlight-induced lipid peroxidation in liposomal membrane. *Radiation Research*, 83:290–302, 1980.

[42] M. Bassas, A. M. Marqués, and A. Manresa. Study of the crosslinking reaction (natural and uv induced) in polyunsaturated pha from linseed oil. *Biochemical Engineering Journal*, 40:275–283, 2007.

[43] Anne-Laure Fameau, Audrey Arnould, and Arnaud Saint-Jalmes. Responsive self-assemblies based on fatty acids. *Current Opinion in Colloid & Interface Science*, 19(5):471–479, 2014.

[44] Irene A Chen and Jack W Szostak. A kinetic study of the growth of fatty acid vesicles. *Biophysical journal*, 87(2):988–998, 2004.

[45] Romain Bordes, Marc Vedrenne, Yannick Coppel, Sophie Franceschi, Emile Perez, and Isabelle Rico-Lattes. Micelle–vesicle transition of fatty acid based ion-pair surfactants: Interfacial evidence and influence of the ammonium counterion structure. *ChemPhysChem*, 8(13):2013–2018, 2007.

[46] Hongguang Li, Stefan A Wieczorek, Xia Xin, Tomasz Kalwarczyk, Natalia Ziebacz, Tomasz Szymborski, Robert Hołyst, Jingcheng Hao, Ewa Gorecka, and Damian Pociecha. Phase transition in salt-free catanionic surfactant mixtures induced by temperature. *Langmuir*, 26(1):34–40, 2010.

[47] Panpan Fan, Yuxian Wang, Jian Shen, Ling Jiang, Wei Zhuang, Yuwang Han, and Hongman Zhang. Self-assembly behaviors of c_{18} fatty acids in arginine aqueous solution affected by external conditions. *Colloids and Surfaces A: Physicochemical and Engineering Aspects*, 577:240–248, 2019.

[48] Jean-Paul Douliez, Bérénice Houinsou Houssou, A-Laure Fameau, Laurence Navailles, Frédéric Nallet, Axelle Grélard, Erick J Dufourc, and Cedric Gaillard. Self-assembly of bilayer vesicles made of saturated long chain fatty acids. *Langmuir*, 32(2):401–410, 2016.

[49] Y. Fan, J. Ma, Y. Fang, T. Liu, X. Hu, and Y. Xia. Neutral and acid-adapted fatty acid vesicles of conjugated linoleic acid. *Colloids and Surfaces B: Biointerfaces*, 167:385–391, 2018.

[50] D. Milshteyn, B. Damer, J. Havig, and D. Deamer. Amphiphilic compounds assemble into membranous vesicles in hydrothermal hot spring water but not in seawater. *Life*, 8:11, 2018.

[51] Nicolas Martin and Jean-Paul Douliez. Fatty acid vesicles and coacervates as model prebiotic protocells. *ChemSystemsChem*, 3(6):e2100024, 2021.

[52] Ye Fan, Yun Fang, and Lin Ma. The self-crosslinked ufasome of conjugated linoleic acid: Investigation of morphology, bilayer membrane and stability. *Colloids and Surfaces B: Biointerfaces*, 123:8 – 14, 2014.

[53] Y. Fan, Y. Fang, Ma L., and H. Jiang. Investigation of micellization and vesiculation of conjugated linoleic acid by means of self-assembling and self-crosslinking. *J. Surfact. Deterg.*, 18:179–188, 2015.

[54] C. F. Bohren and D. R. Huffman. *Absorption and Scattering of Light by Small Particles*. Wiley, New York, NY, 1998.

[55] J. Bertolotto, M. Perez Reale, and M. Bergonzi Rodriguez. DeterminaciÓn del tensor polarizabilidad Óptica del adn tipo varilla. *ANALES AFA*, 11(1), 2013.

[56] P. Y. Liu, L. K. Chin, W. Ser, H. F. Chen, C.-M. Hsieh, C.-H. Lee, K.-B. Sung, T. C. Ayi, P. H. Yap, B. Liedberg, K. Wang, T. Bourouina, and Y. Leprince-Wang. Cell refractive index for cell biology and disease diagnosis: past, present and future. *Lab Chip*, 16:634–644, 2016.

[57] Ramon D. Wolstencroft. Terrestrial and Astronomical Sources of Circular Polarisation: A Fresh Look at the Origin of OF Homochirality on Earth. In R. Norris and F. Stootman, editors, *Bioastronomy 2002: Life Among the Stars*, volume 213, page 154, June 2004.

[58] Iván Lechuga and Karo Michaelian. Fatty acid vesicles as hard uv-c shields for early life. *Foundations*, 3(1):99–114, 2023.

[59] Bettina E. Schirrmeister, Patricia Sanchez-Baracaldo, and David Wacey. Cyanobacterial evolution during the precambrian. *International Journal of Astrobiology*, 15(3):187–204, 2016.